Article

Unveiling the Impact of Aggregation on Optical Anisotropy of Triazaacephenanthrylene Single Crystals. A Combined Quantum Crystallography and Conceptual Density Functional Theory Approach

Published as part of The Journal of Physical Chemistry virtual special issue "Paul Geerlings Festschrift".

Marlena Gryl,* Katarzyna Ostrowska, Jose Enrique Barquera-Lozada, and Katarzyna M. Stadnicka

Cite This: *J. Phys. Chem. A* 2020, 124, 2931−2941

Read Online

ACCESS | Metrics & More | Article Recommendations | Supporting Information

ABSTRACT: Triazaacephenanthrylene (TAAP) triclinic single crystals show substantial optical anisotropy of absorption and fluorescence. The maximum effect can be correlated with the direction perpendicular to the plane of chromophores connected in a head-to-tail manner via weak dispersive interactions. This phenomenon is uncommon as usually the existence of postulated $\pi\cdots\pi$ interactions between the molecules forming dimers or stacks cause quenching of fluorescence. Herein we present a comprehensive study of inter- and intramolecular interactions in the crystal of TAAP enriched with the investigation of aromaticity. Our results show that intramolecular interactions stabilize the overall conformation of the molecule whereas dispersive forces determine the aggregation between TAAP molecules. In fact, there is no conventional $\pi\cdots\pi$ interaction between the molecules in the dimer. Instead, we observed a close contact between the lone pair of the bridgehead N10B atom and π-deficient pyrazine ring from an adjacent molecule. Optical anisotropy in TAAP crystals was directly correlated with the alignment of the molecular transition dipole moments caused by specific molecular self-assembly.
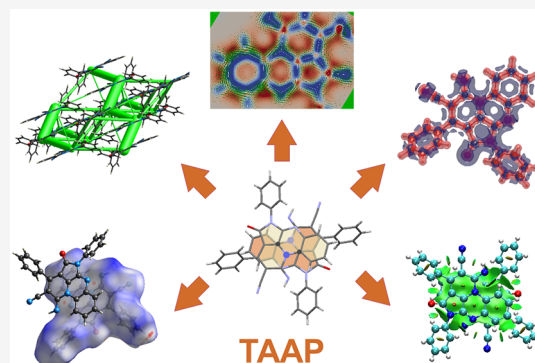
INTRODUCTION

The relative orientation of building blocks in a crystal structure can strongly influence the magnitude of the obtained physical effect.[1−4] Properties such as birefringence, second harmonic generation, pyro-piezoelectricity, or elastic properties are guided by crystal symmetry and, as such, are expected to differ when measurement directions are changed in a crystalline solid. The degree of anisotropy depends on the molecules used to construct the solid in question.[5−10] Understanding weak interactions between molecules in those cases plays a key role in the design of materials with programmed properties. From the crystal engineering paradigm we know that the first interactions that appear in the solid state are intramolecular ones, forming six-membered rings through the intramolecular hydrogen bond.[11,12] In the next step, intermolecular strong and moderate interactions are created by using the remaining good donor and acceptor sites. In this case the influence of directional interactions such as hydrogen or halogen bonds on the relative orientation of molecular building blocks is undeniable.[13,14] The situation is more complicated when we are dealing with molecules capable of forming only weak and/or strongly dispersive interactions

with neighboring building blocks.[15,16] The question remains open: what is the influence of the electronic properties of a single molecule on the aggregation and what happens when there are no strong nor moderate directional forces guiding the molecular recognition. Among those weakly bonded systems conjugated molecules with multiple aromatic or weakly aromatic rings are the most challenging. In those cases separating the influence of a particular interaction on the obtained crystal packing seems to be close to impossible despite a few successful cases.[17] In the recent years the need to examine interactions such as $\pi\cdots\pi$, anion$\cdots\pi$, cation$\cdots\pi$, or lone pair$\cdots\pi$ increased, giving rise to intensive research toward recognition of their nature.[18−20] Some of them, e.g., $\pi\cdots\pi$ interactions, are known to be dispersive, the nature of others like C−H$\cdots\pi$ or cation/anion$\cdots\pi$ is still under scientific
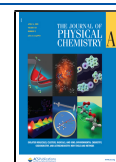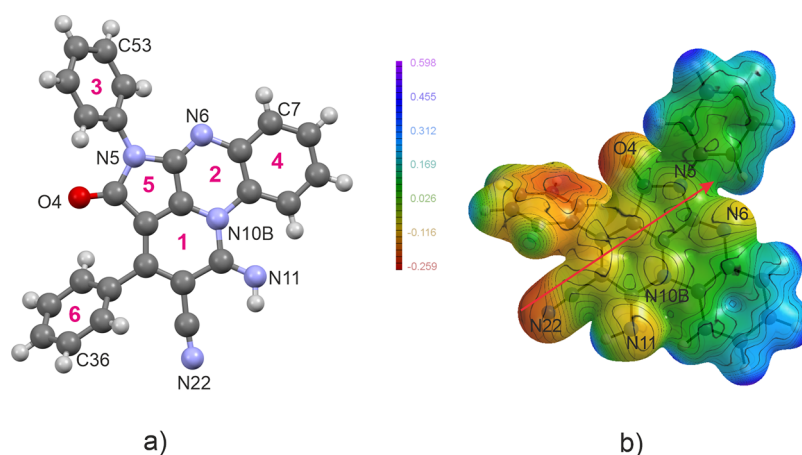
Figure 1. (a) Contents of the asymmetric unit of TAAP with atom and ring numbering schemes. (b) ESP plotted on the 0.1 e Å^{-3} electron density isosurface obtained from experimental data. Black arrow marks the direction of the dipole moment calculated for the isolated molecule.

debate.[21−23] The strength of $\pi\cdots\pi$ interactions is known to depend on the superposition of aromatic systems. Among the π-stacked systems the most favorable orientation is the one with significant offset geometry. In this case $\pi\cdots\sigma$ attraction dominates over $\pi\cdots\pi$ repulsion.[24] Spectral properties such as absorption and emission, both in solid state and in solutions, are strongly influenced by the formation of those weak interactions.

In this manuscript we make an attempt to understand the driving force behind the aggregation associated with the formation of weak, disperse in nature, interactions. For this reason we have chosen a triazaacephenanthrylene chromophor (TAAP).[25] Our previous studies on TAAP showed unusual absorption and fluorescence anisotropy with the maximum fluorescence observed in the direction of postulated $\pi-\pi$ interactions in the crystal. In the current literature concerning the origin of fluorescence in organic materials there is a general opinion that fluorescence is always quenched in the direction of $\pi-\pi$ interaction.[26,27] The concomitant absorption and fluorescence anisotropy in the crystals of TAAP makes this system unique in terms of intramolecular interactions contributing to the directionality of the properties. Here we will use experimental and theoretical quantum crystallography tools[28] such as electron density studies (multipolar formalism[29] and quantum theory of atoms in molecules (QTAIM)[30]), Hirshfeld surfaces, and energy framework assessment[31] combined with the conceptual density functional theory (DFT) descriptors of aromaticity[32] and energy decomposition analysis[33] to unveil factors that influence the unusual optical properties of TAAP crystals.

MATERIALS AND METHODS

Synthesis and Crystallization. The material, 5,6,10b-triazaacephenanthrylene (TAAP), analyzed in this manuscript is closely related to many naturally occurring bioactive compounds, e.g., aristolactams exhibiting photoconductance, photochemical, and electroluminescent properties.[34] Details of the synthesis,[35] conventional crystal structure analysis, and optical properties (absorption and fluorescence)[26] can be found in our recent published articles. TAAP contains conjugated pyrazine and pyridine rings fused with the benzene and pyrrol-2-one ones. X-ray diffraction analysis showed coplanarity of heterocyclic rings and conjugation of 12-π electron system with two electron pairs located at bridgehead

nitrogen atom N10B and amide nitrogen atom N5. The compound was crystallized from THF, CHCl$_3$, tetrachloroethane-d_2, toluene, dioxane, acetonitrile, or the mixture acetonitrile−water. In all cases the obtained crystals were centrosymmetric with the space group $P\bar{1}$ and the same lattice parameters. The isolated molecule of TAAP (Figure 1a) has a dipole moment of 3.82 D; however, in the crystal structure the molecules form centrosymmetric dimers (Figure S1), with resultant dipole moment equal to zero. Attempts of TAAP cocrystallization (different conditions/methods) using complementary building blocks (such as benzoic acid, quinoline, phenol, etc.) always yielded crystals of TAAP substrate. This unusual stability of the dimeric system required further examination with an emphasis placed on the following aspects: nature and strength of intermolecular interactions in the dimers as well as the character and strength of interactions connecting the dimers in the solid state.

Electron Density and Weak Interactions Analysis. The wavefunctions for QTAIM calculations in AIMAll[36] were obtained from Gaussian16[37] at the M052X/6-311+G(2df,2p) level of theory both for an isolated molecule of TAAP and for the dimer. M052X/6-311+G(2df,2p) allows a reliable description of weak, dispersive interactions in the dimeric systems.[38] Monomer and dimer geometries were taken from the optimized in-crystal geometry with Crystal17[39,40] using PB3LYP/POB-TZVP. Bader's theory of atoms in molecules[30] was used for assessment of intramolecular and interdimer interactions. Those results were compared with the topological analysis of electron density within TAAP crystal.

Experimental electron density was obtained from multipolar refinement using Hansen−Coppens formalism implemented in XD2016.[41] An experimental high resolution (up to $\sin\Theta/\lambda$ = 1.0976 Å^{-1}, Θ_{max} = 51.27°) and low temperature (90 K) data set was collected on a Rigaku XtaLAB Synergy-S with a HyPix-6000HE detector and a dual microfocus (Cu/Mo) X-ray diffractometer equipped with Cryostream 800 Plus. Theoretical structure factors were generated for the in-crystal geometry (Crystal17,[39,40] PB3LYP/POB-TZVP) obtained from the experimental multipolar refinement and kept fixed in the subsequent refinement on theoretical data (Table S1). Details of the multipolar refinement including the choice of local symmetry and discussion of residual density analysis,[42] which confirmed the correctness of the assumed model, was shown in the Supporting Information. The ESP was plotted on the

electron density isosurface obtained from experimental data (Figure 1b) as well as from theoretical models (Figure S2). Kinetic energy densities were estimated according to Abramov approach,[43] and interaction energies for weak interactions both in the dimer and in the crystal structures were calculated assuming Espinosa approximation.[44] NCI analysis[45,46] was employed to visualize and analyze interactions between the dimers as well as interactions combining dimeric aggregates. Hirshfeld surfaces, fingerprint plots, interaction energies, and energy framework visualization were all performed using CrystalExplorer17.[31] Energy frameworks and interaction energies were calculated in CrystalExplorer at the available B3LYP/6-31G(d,p) level.

Energy Decomposition Analysis. Ziegler−Rauk energy decomposition analysis[47] was carried out on the PB3LYP/POB-TZVP optimized structures using PBE/TZ2P+ in ADF2019.[48−50] Dispersion was accounted for using Grimme's revised DFT-D3 approach.[51] This particular choice of basis set/functional has proven to be accurate for studying weak interactions including those dispersive in nature.[52] The total interaction energy between the monomers was expressed as a sum of dispersion energy E_{disp}, Pauli repulsion E_p, electrostatic interaction E_{es}, and orbital interaction E_{oi} and it was corrected for the BSSE error (E_{BSSE}).

Aromaticity. Multicenter bond indices I_{ring} and MCI were calculated for all six-membered and five-membered rings both in the isolated molecule and in the dimer to assess their aromaticity. Computations were performed in ADF2019[48−50] at the PBE/TZ2P+ level with dispersion introduced with Grimme's revised DFT-D3 approach.[51] I_{ring} and MCI are both derived from electron delocalization description of aromaticity and were proven useful in discriminating relative aromaticity in polycyclic compounds. I_{ring} defined by Giambaggi and coworkers[53] takes into consideration the Kekulé model whereas MCI[54] also takes into account other possible arrangements of atoms in a ring. Usually, the two indices give similar results as the Kekule model is proving to give the largest contribution to the aromaticity description.[55] The values of those two indices were compared with the results obtained via analysis of the vorticity of the current density. The geometry of the monomer and dimer of TAAP were optimized using M06/Def2-TZVP with empirical dispersion corrections, which has proven to be adequate for vorticity studies in weakly bonded systems.[56,57] The magnetically perturbed wavefunctions were obtained using gauge-including atomic orbitals. These calculations where performed with Gaussian16.[37] The software AIMAll was used to calculate the magnetically induced current density, $J(r)$, vector field.[36] The magnetic field, **B**, is perpendicular to the molecular plane. The triple product of the current density, $tpJ(r)$, scalar field and the circulation, C, were calculated numerically with a set of python scripts.[57,58] These scripts use the pvpython library included in Paraview 5.2. The loop for the calculation of C is the geometric structure of the molecular ring at 1.0 bohr from the molecular plane. Aromaticity calculations gave an added value to the description of the interacting molecules.

■ RESULTS AND DISCUSSION

Aromaticity of TAAP. Schematic representation of TAAP molecule as seen in the asymmetric part of the unit cell is presented in Figure 1a. The core of the molecule, triazaacephenanthrylene, is built from four fused rings: pyridine (1), pyrazine (2), benzene (4) and pyrrol-2-one

(5), among which three are heterocycles with three nitrogen atoms N6, N10B, and N5. Additionally there are two phenyl substituents on each side of the C4−O4 carbonyl bond: rings (3) at N5 and (6) at C3. Analysis of multicenter bond indices[53,54] (Table 1) revealed that phenyl rings (3) and (6)

Table 1. Aromaticity Indicators I_{ring} and MCI for TAAP Isolated Molecule

ring	I_{ring}	MCI	atoms
(1)	0.008	0.010	C1 C2 C3 C3A C3A′ N10B
(2)	0.007	0.008	C3A′ C5A N6 C6A C10A N10B
(3)	0.043	0.063	C51 C52 C53 C54 C55 C56
(4)	0.032	0.046	C6A C7 C8 C9 C10 C10A
(5)	0.011	0.009	C3A′ C3A C4 N5 C5A
(6)	0.043	0.063	C31 C32 C33 C34 C35 C36

are aromatic, with indicators comparable to those of naphthalene rings. Among the fused rings benzene (4) is still aromatic, whereas azaarenes pyridine (1), pyrazine (2), and pyrrol-2-one (5) have I_{ring} values much lower than the cutoff for aromatic systems (0.017), which shows their π-deficient character. As it could have been expected, the aromatic rings are in fact the phenyl ones outside the chromophore and the benzene ring (4) fused in quinoxaline system, whereas the aromaticity of the fused heterocyclic system decreases with respect to the isolated rings. The aromaticity indicators do not change significantly when moving from the monomer to the dimer (see Table S2).

Recently, it was proposed that the aromaticity of the individual rings of polycyclic compounds can be effectively evaluated with the circulation (C) of the magnetically induced current density $J(r)$.[57] The circulation is the surface integral of triple product $B\cdot\nabla \times J(r)$ ($tpJ(r)$), which is a scalar field that indicates the diatropic (negative) and paratropic (positive) regions in a molecule. Diatropicity has been extensively related with aromaticity, while paratropicity with antiaromaticity.[59−62] Large negative regions of $tpJ(r)$ above the molecular plane and large negative values of C indicate a strong diatropicity of a ring, while large positive values indicate strong paratropicity. If C is close to zero the magnetic induced currents are weak, which is characteristic for nonaromatic compounds. We have performed calculations of $tpJ(r)$ and C for the isolated TAAP and for its dimer. According to C, only benzene ring (4), fused with the heterocyclic system of TAAP, is truly aromatic (strong diatropicity, Figure 2). Pyrazine ring (2) is only slightly
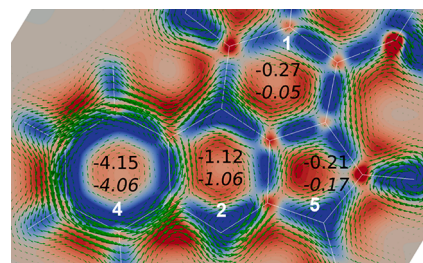

Figure 2. $tpJ(r)$ contour map of TAAP. Ring numbering scheme in white. Color code: $\leq -0.8 \times 10^{-3}$ au (dark blue), 0.0 au (white), and $\geq 0.8 \times 10^{-3}$ au (red). The plane is parallel to the molecule at 1.0 bohr from it. The values of C for individual rings of the monomer (normal) and the dimer (cursive) in 10^{-4} au. $J(r)$ vectors are displayed as green arrows.
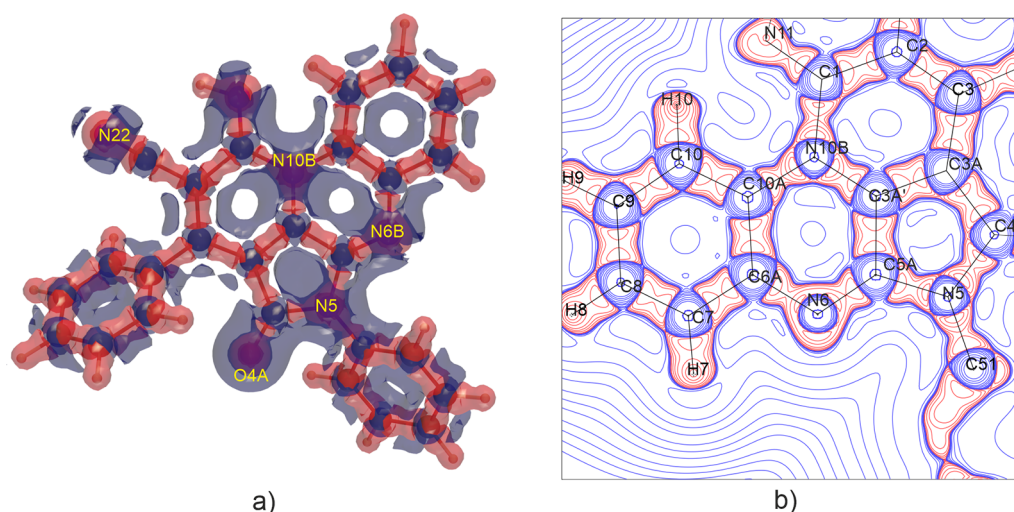
Figure 3. (a) 3D Laplacian of electron density. Isosurfaces drawn at −0.2 au (red surface) or +0.2 au (blue surface). Figure prepared in DrawMol software.[64] (b) Laplacian contour map in the C10A−C3A′−N10B plane. Contours are at logarithmic intervals in $-\nabla^2\rho(r)$ e Å^{-5} [(±2, 4, 8) × 10^n e Å^{-5}, where n $-3 \leq n \leq 3$].
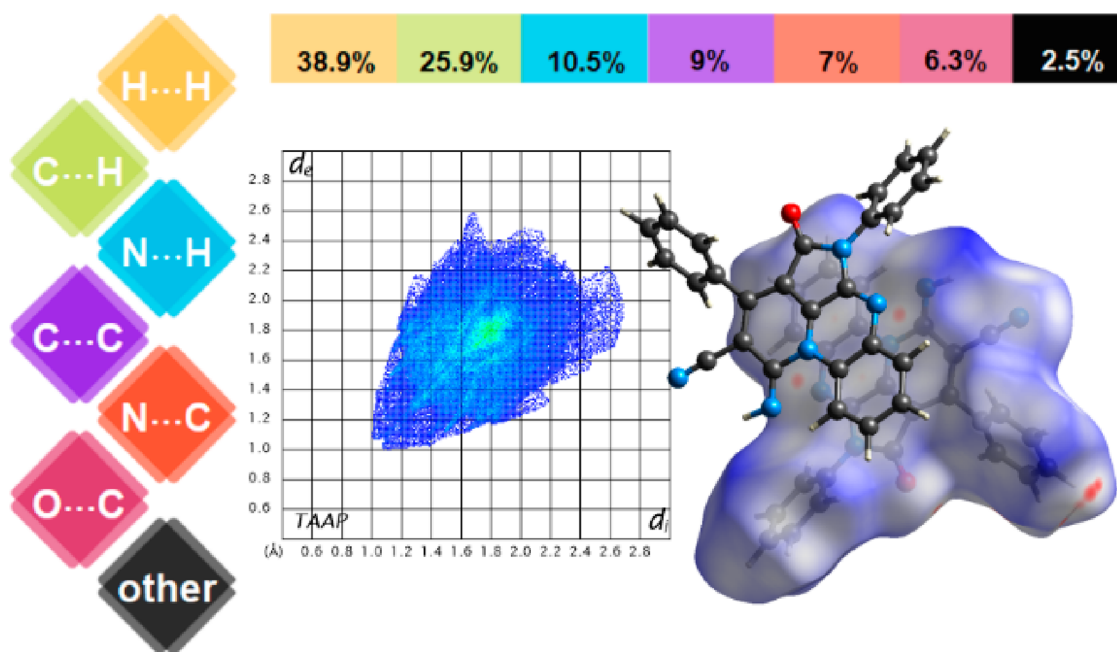

Figure 4. Fingerprint plot for TAAP with percent of the interaction in the crystal (left). Hirshfeld surface showing only very weak interactions between molecules in the dimer (right).

aromatic, while rings (1) and (5) are nonaromatic. Figure 2 also shows that around benzene ring (4) there is a strong diatropic electronic current (green arrows). It is worthwhile to note that the aromaticities of the rings do not change significantly in the dimer, despite the slight geometric changes (see Table S3).

Topological Analysis of Electron Density. Topological analysis of electron density was performed in order to reveal the factors contributing to the molecular recognition in the TAAP structure. Calculations were conducted first for the isolated molecule of TAAP (optimized and experimental geometries) and then on the centrosymmetric dimer (optimized in B3LYP/TZVP). The results obtained in this way were then compared with multipolar refinement models derived from experimental data and calculated using theoretical

structure factors (Crystal17, PB3LYP/POB-TZVP). The chemical character of the TAAP fused ring system was examined using the electrostatic potential (ESP) plotted on the electron density isosurfaces for isolated molecule (Figure 1b) and the one present in crystal (Figure S2). The ESP clearly indicates the nucleophilic and electrophilic regions in this molecule. The most negative electrostatic potential can be observed for oxygen atom O4 and nitrogen atom N22. The decrease of the ESP was found for nitrogen atoms N10B, N6, and N11 (compare Figure 1b). Here N11 is the acceptor of the intramolecular hydrogen bond (C10−H10···N11). The slightly negative potential for N10B values coincided nicely with a slightly positive value found in the center of pyrazine ring (2). The ESP distributions within the isolated molecule, in the dimer and in theoretically determined ED, are similar. There is
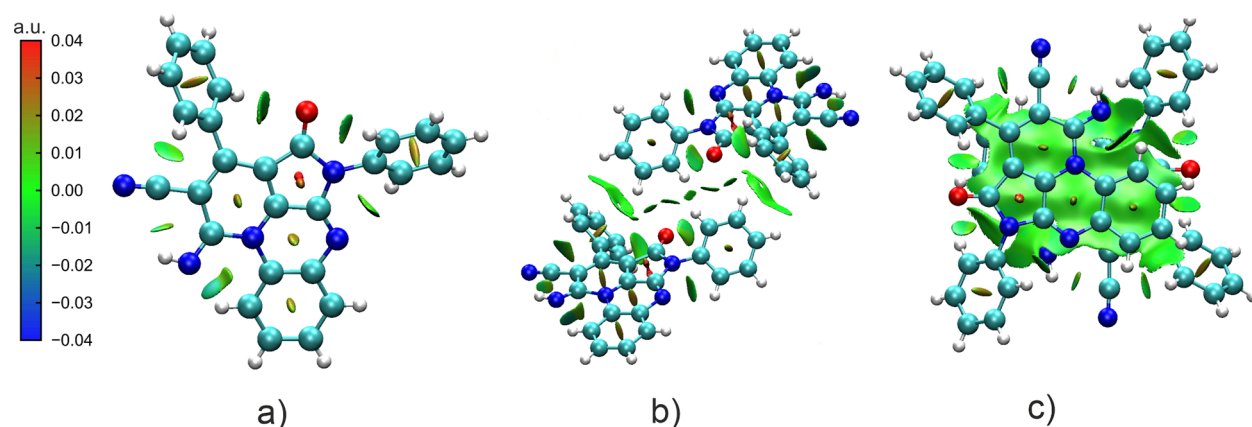
Figure 5. Reduced gradient of electron density plotted for (a) an isolated molecule of TAAP, (b) two molecules interconnecting the dimers in 3D architectures, and (c) a dimer in the crystal of TAAP. Calculations performed in NCIplot. The gradient cutoff was set to 0.5 au.

Table 2. Experimental Topological Analysis of Bond Critical Points for Selected Weak Interactions in TAAP[a,b]

	d_1	d_2	$\rho(r)$	$\nabla^2\rho(r)$	$G(r_{CP})$	$V(r_{CP})$	$E(r_{CP})$	$|V(r_{CP})|/G(r_{CP})$	$E(r_{CP})/\rho(r)$	$G(r_{CP})/\rho(r)$	E_{int}
H10···N11	0.809	1.263	0.170	2.260	0.150	−0.140	0.010	0.933	0.059	0.882	−6.509
	0.807	1.266	0.170	2.400	0.160	−0.140	0.020	0.875	0.118	0.941	−6.509
N6···N11[i]	1.565	1.678	0.050	0.680	0.040	−0.030	0.010	0.750	0.200	0.800	−1.395
	1.562	1.684	0.050	0.690	0.040	−0.030	0.010	0.750	0.200	0.800	−1.395
H33···O4[ii]	1.100	1.441	0.050	0.830	0.050	−0.030	0.020	0.600	0.400	1.000	−1.395
	1.094	1.462	0.050	0.770	0.040	−0.030	0.010	0.750	0.200	0.800	−1.395
C33···C33[ii]	1.475	1.475	0.060	0.630	0.040	−0.030	0.010	0.750	0.167	0.667	−1.395
	1.475	1.475	0.050	0.590	0.030	−0.030	0.000	1.000	0.000	0.600	−1.395
N22···N10B[iii]	1.563	1.595	0.050	0.650	0.040	−0.030	0.010	0.750	0.200	0.800	−1.395
	1.557	1.601	0.050	0.660	0.040	−0.030	0.010	0.750	0.200	0.800	−1.395
H32···N11[iii]	1.518	1.563	0.050	0.610	0.030	−0.030	0.000	1.000	0.000	0.600	−1.395
	1.538	1.573	0.050	0.590	0.030	−0.020	0.010	0.667	0.200	0.600	−0.930
H10···C33[iii]	1.227	1.733	0.040	0.450	0.020	−0.020	0.000	1.000	0.000	0.500	−0.930
	1.223	1.751	0.040	0.450	0.020	−0.020	0.000	1.000	0.000	0.500	−0.930
H8···H36[i]	1.493	1.322	0.030	0.400	0.020	−0.020	0.000	1.000	0.000	0.667	−0.930
	1.532	1.324	0.030	0.370	0.020	−0.010	0.010	0.500	0.333	0.667	−0.465
C21···C1[iii]	1.654	1.689	0.040	0.490	0.030	−0.020	0.010	0.667	0.250	0.750	−0.930
	1.655	1.682	0.040	0.500	0.030	−0.020	0.010	0.667	0.250	0.750	−0.930
C3A′···C10A[i]	1.699	1.700	0.040	0.420	0.020	−0.020	0.010	1.000	0.250	0.500	−0.930
	1.698	1.703	0.040	0.430	0.020	−0.020	0.010	1.000	0.250	0.500	−0.930

[a] d_1, d_2 = distance between BCP and atoms 1 and 2, respectively (Å). $\rho(r)$/e Å^{-3} = charge density. Laplacian = $\nabla^2\rho(r)$/e Å^{-5}, $G(r_{CP})$/hartrees Å^{-3}, $V(r_{CP})$/hartrees Å^{-3} local kinetic and local potential energy density, respectively. $E(r_{CP})$/hartrees Å^{-3} = local energy density of the electrons. E_{int} was estimated using approach described in Espinoza et al.[58] [b] i: −x + 2, −y, −z + 1. ii: 1 − x, 1 − y, 2 − z. iii: 2 − x, 1 − y, 1 − z.

a slight difference in the ESP when the center of phenyl ring (6) from experimental electron density and theoretical data are compared (Figure S2). This is not entirely surprising that the theoretical model differs from the experimental one, as for example, it does not take into account thermal displacement of electron density. The distribution of the ESP in the molecule interplays with the direction of the dipole moment (marked in red on Figure 1b). Topological properties at the bond critical points for all covalent bonds found in TAAP are shown in Table S4. There are only small variations in the values of electron density at the BCP for the covalent bonds with the largest values obtained from experimental data set. The values of $\nabla^2\rho(r)$ and λ_3 change more significantly. In particular we can observe a systematic increase of λ_3 of C−N and C−C bonds when moving from the isolated molecule and dimer to the crystal environment. The only exception is the C21−N22 bond where λ_3 increases almost doubly (from around 25e/A^5 up to ca. 47 e/A^5). The observed value of ε for this bond is

close to zero, which confirms its triple character. A similar situation can be observed for the carbonyl C4−O4 bond, which has a double character. The increase in λ_3 values and more positive values of the $\nabla^2\rho(r)$ indicates, in general, more dissipated electron density toward the position of the nuclei associated with the polar character of the bond. However, the magnitude of the effect is directly related with the misfit between theory and experiment. Such an effect is not uncommon when dealing with covalent polar multiple bonds, where the Laplacian and λ_3 values can change dramatically between experimental and theoretical data as a result of only slight shift of BCP position.[63] The Laplacian maps in the plane of C5A−C6A−N10B and the 3D isosurface are shown in Figure 3. The 3D representation of the Laplacian of electron density clearly indicates lone pairs located at nitrogen atoms N5 and N10B positioned out of plane of the fused ring system. The geometrical analysis and in particular the examined overlap of the fused systems in the dimer showed that atom
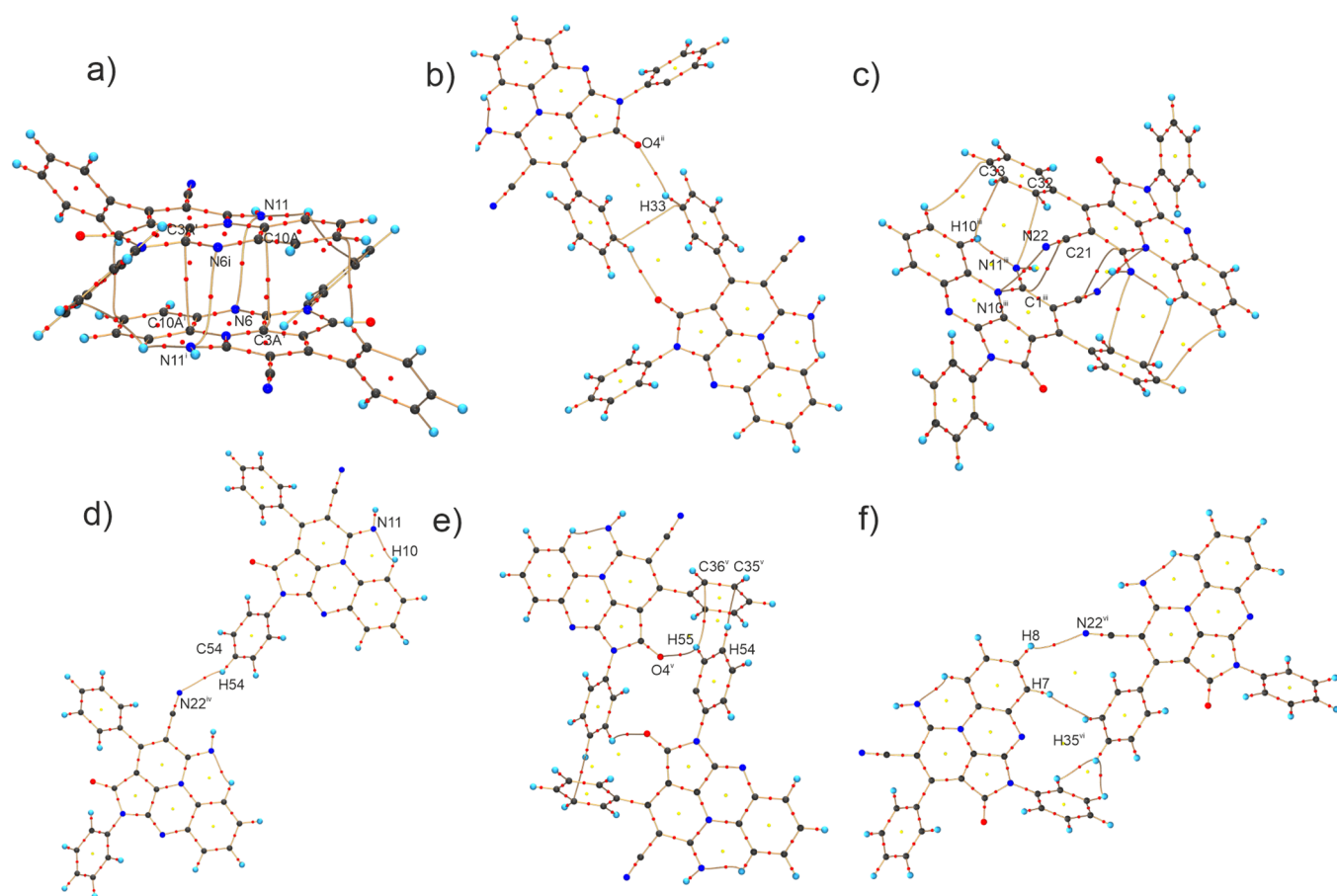
Figure 6. Molecular graphs of TAAP with marked BCP for weak intermolecular interactions.
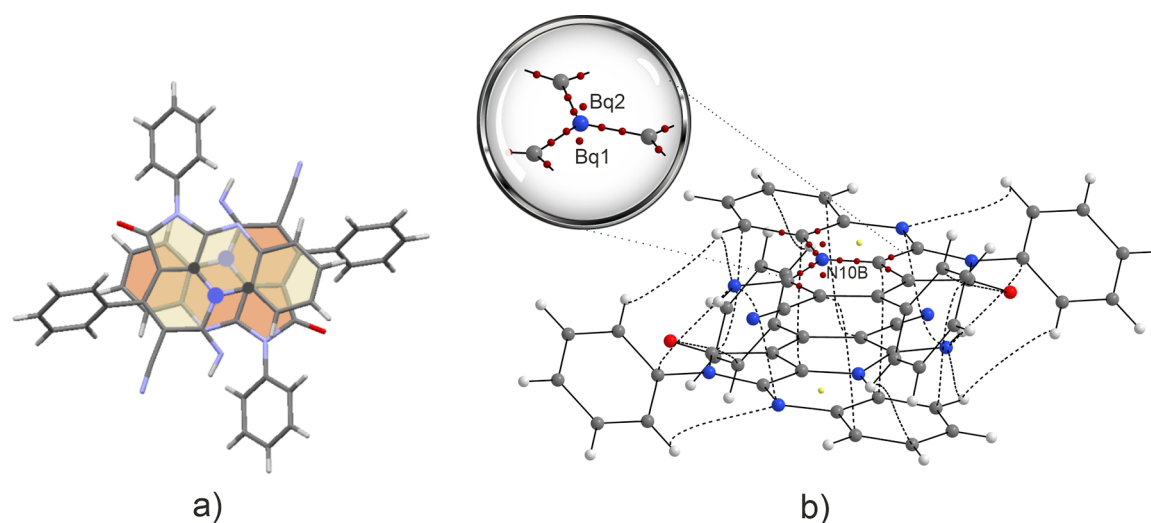

Figure 7. (a) Overlap between the TAAP fused rings with marked key contact points on the two C10A and C3A′ atoms (gray) and between N10B and the center of the pyrazine ring of an adjacent molecule (blue). (b) VSCC calculated for the N10B atom with marked nonbonding maxima.

N10B was located in the close vicinity of the center of adjacent pyrazine ring (2).

This information, together with the weakly aromatic character of the pyrazine ring (according to C values, Figure 2) forced us to examine interactions between the dimer in more detail.

Weak Interactions. At first we performed geometrical analysis by means of Hirshfeld surface and fingerprint plots

(Figure 4). It is obvious at first glance that H···H and C···H contacts are predominantly present in the crystal. Other significant contributions come from N···H, C···C, C···N, and C···O contacts. This scheme confirms the impact of weak interactions on the overall packing in the crystal structure of TAAP.

The noncovalent interaction index (NCI) based on the analysis of reduced gradient of electron density was used to

Table 3. Interaction Energy for the TAAP Dimer Calculated Using Conceptual DFT Approach (TAAP dimer ADF), Using Dimer in the Crystal Environment (TAAP Dimer XD) and a Dimer Embedded in Cluster around a Central Molecule in Question of 3.8 Å (TAAP dimer CrystelExplorer)[a]

	ΔE_{Pauli}	ΔE_{OI}	ΔE_{es}	ΔE_{disp}	ΔE_{int}	$\Delta E_{intBSSE}$
TAAP dimer ADF	17.99	−6.07	−10.22	−21.61	−19.91	−17.65
N-CH$_3$ pyrazine dimer ADF	20.08	−11.05	−12.75	−7.29	−11.01	−10.07
pyrazine dimer ADF	4.51	−1.35	−1.76	−3.65	−2.25	−1.75
	ΔE_{ex-rep}		ΔE_{es}	ΔE_{disp}	ΔE_{int}	
TAAP dimer XD	60.00		−23.57	−58.15	−21.54	
	ΔE_{Rep}	ΔE_{Pol}	ΔE_{es}	ΔE_{disp}	ΔE_{int}	
TAAP dimer CrystalExplorer	19.4	−1.12	−3.54	−32	−20.46	

[a]For comparison purposes interaction energies of pyrazine and N-methylpyrazine dimers with the same geometries of the rings were added.
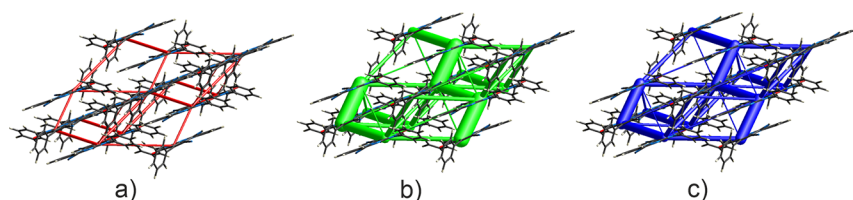

Figure 8. Energy frameworks calculated for the cluster of 3.8 Å around the central molecule: (a) red, electrostatic contribution; (b) green, dispersion; (c) blue, total energy. The largest cylinders represent the strongest interaction between the molecules forming a dimer. The tube size was selected as 80 and a cutoff value is 5 kJ/mol.

visualize particular interactions contributing to the overall crystal packing (Figure 5). In the studied system we can recognize several weak intramolecular interactions marked in the NCIplot as green irregular surfaces. Among them only C10−H10···N11 can be considered a weak hydrogen bond with the energy ca. −6.5 kcal/mol (QTAIM analysis, Table 2). The intramolecular hydrogen bond and the remaining weak interactions within this molecule stabilize the overall conformation of the TAAP (Figure 5a). This situation is consistent both for isolated molecules and isolated dimer and for the dimer in the crystal. Molecules in the dimer are connected via dispersive interactions (Figure 5c) formed between the three fused heterocyclic π-deficient rings (1), (2), and (5). The adjacent molecules in the structure are also connected via weak, dispersive in nature forces. (Figure 5b).

QTAIM analysis for the crystal of TAAP revealed two pairs of symmetric bond paths and corresponding BCPs formed between the C3A′···C10A[i] and N6···N11[i] (i: −x + 2, −y, −z + 1) atoms connecting two molecules in the dimer (Figure 6a). Neighboring molecules from two adjacent dimers are interconnected by the C33−H33···O4[ii] (ii: 1 − x, 1 − y, 2 − z) bond in [011] (Figure 6b) and by several other weak interactions including the one between the C21−N22 group and C1−N10B close to the [110] direction (Figure 6c). In the structure there are additional C−H···N and C−H···O interactions (Figure 6d−f) as well as C−H···π interactions between the two neighboring phenyl rings (3) and (6) (Figure 6e). On the basis of the analysis of BCPs and bond paths there is no evidence of direct interaction between N10B and the C3A′C5AN6C6AC10AN10B pyrazine ring, despite their close proximity.

In order to examine this potential N10B weak lone pair···π-deficient pyrazine ring interaction further we have performed calculations of valence shell charge concentrations (VSCC) for N10B and adjacent carbon atoms C1, C3A′, and C10A in the dimer (Figure 7a). There are three bonding maxima associated with the N10B atom and correlated with the three covalent

bonds formed between this atom and the above-mentioned carbon atoms. Additionally, we have two nonbonding maxima, one above and one below the plane formed by pyrazine ring. The bottom one (marked Bq$_1$) is pointing directly to the center of the electron-deficient pyrazine ring located below. The differences between Bq$_1$ and Bq$_2$ in terms of electron density are small (3.228 and 3.206 e/Å^3, respectively). In the monomer the respective values are 3.213 and 3.206 e/Å^3.

Interaction Energies. Table 2 presents topological properties evaluated at the BCPs for selected weak interactions in the TAAP crystal structure (full data for all interactions available in Si file). Analysis of electron density and its Laplacian, local kinetic and potential energy densities, and derived from them interaction energies (E_{int}) calculated using Abramov approximation allowed to hierarchize interactions. We can classify all the hydrogen bonds in this structure as pure closed shell ($\nabla^2\rho(r) > 0$, $|V(r_{CP})|/G(r_{CP}) < 1$, and $E(r_{CP})/\rho(r) \geq 0$). From all the interactions in TAAP, those existing within the dimer were selected and summed up, giving −21.54 kcal/mol (TAAP dimer XD). This value was confronted with the energies calculated for the TAAP dimer using conceptual DFT approach and a dimer embedded in cluster or nearest neighbors around a central molecule in question.

Using established hierarchy of interactions, we were able to reconstruct crystal structure assembly by the analysis of possible molecular recognition schemes and assuming crystal engineering paradigm.

First an intramolecular hydrogen bond C10−H10···N11 is formed, closing a six-membered ring. At the next stage a dimer between adjacent TAAP molecules is created. The total energy of the dimer was estimated to be around −20 kcal/mol (averaged value assessed from those marked green in Table 3), which makes it a predominant interaction in this system. For comparison purposes and to understand the large interaction energies observed for this type of dimer, we have analyzed similar interactions (retaining the same geometry) within pyrazine and N-methylpyrazine dimers. In the pyrazine itself
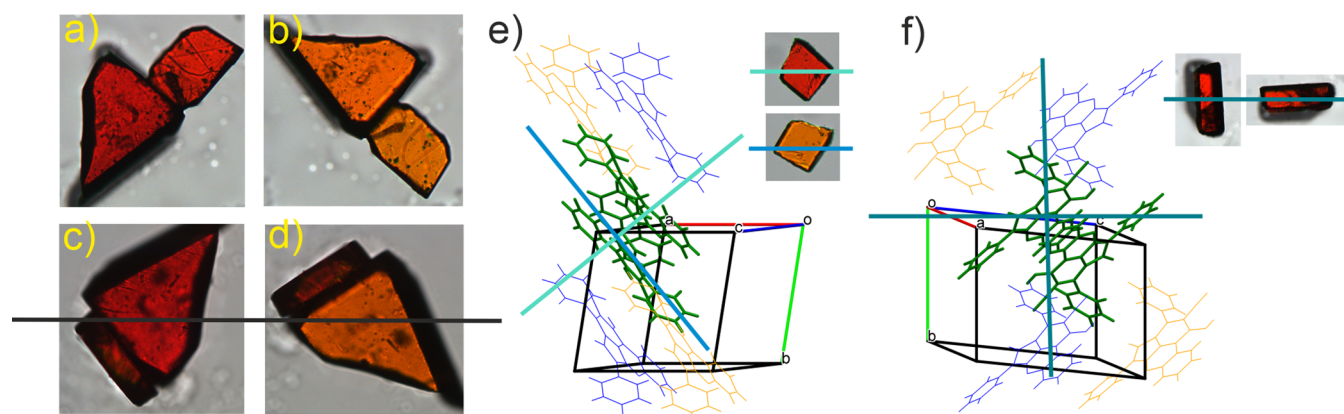
Figure 9. (a)−(d) Crystals of TAAP under polarizing light with marked direction of polarization, (e) view of the (001) face of the crystal and a projection of unit cell onto (001) plane with marked polarization directions blue and green connected with the absorption directions marked on the crystal, (f) view of the (100) face of the crystal with marked polarization directions. Molecules marked in green form a dimer at $(1, 0, \frac{1}{2})$, whereas the blue and yellow ones represent the subsequent aggregation of molecules as seen in the crystal structure.

the electron lone pair of the nitrogen atom is at the hybridized sp^2 orbital in the ring plane with π-deficiency at its center, as a result there is only a weak interaction between the molecules forming the dimer (−1.75 kcal/mol), whereas, in the N-methyl derivative of pyrazine, the electron lone pair of the N-substituted atom is directed toward the center of π-deficient adjacent ring forming the dimer. As a result there is a larger stabilization of such a system (−10.07 kcal/mol). In our case N10B is expected to have properties similar to those of the methyl substituted nitrogen atom in N-methylpyrazine.

It is worthwhile to note that a variety of methods used to obtain this result gave a similar total value of the interaction energy, although the relative contributions of stabilizing and destabilizing forces were different. At the next stage adjacent dimers are connected in two ways: via C33—H33···O4 interactions and using an interaction between nitrile group C21≡N22 and atoms N10 and C1 from pyridine ring. A more descriptive image is provided in Figure 8 showing energy frameworks. Energies between molecular pairs were represented as colored cylinders with radius proportional to the magnitude of each interaction energy. Three types of forces were visualized: dispersive (green), electrostatic (red), and total interaction energy (blue). From Figure 8 it is clear that the molecular recognition in TAAP is dominated by dispersive interactions, starting from the formation of the dimer. This has a profound impact on the properties of the obtained material, as we have proven in our recent work.[25]

Structure−Property Relationship. TAAP exhibits strong anisotropy of absorption and fluorescence on the (001) face of the crystal. In this work we have examined (100) and (010) crystal faces under a polarizing microscope to establish a direct relation between the observed in the solid state interactions and the pleochromism. Those results were confronted with experimental UV−vis spectra measured for the solid state sample of TAAP (Figure S5).

Figure 9a−d shows crystals of TAAP in different orientations, the polarization direction is marked with a black line. Both crystals in Figure 8a,b have (001) faces exposed, whereas on Figure 8c,d the smaller crystal has a (100) face exposed. It is obvious from the colors of the crystals that the pleochroic phenomenon is more profound on the (001) planes; however, it does not disappear completely on the (100) face. Observation in the b^* direction did not give a clear

distinction whether the absorption changes with the orientation, as on this side the crystal has two smaller, narrow, inclined faces. It is known that the absorption anisotropy can be explained by the relative orientations of the largest transition dipole moments (TDMs) of the molecules building the crystal. In our previous paper[25] we have determined the direction of the transition dipole moments for the monomer and dimer of TAAP. All TDMs were found in the plane of the chromophore approximately along the $[\bar{1}10]$ direction, except for one in the dimer and one in the monomer, which were perpendicular to the molecular plane. Those two transition dipole moments (one in the dimer and one in the monomer) can be related with green absorption (red color of the crystal). The remaining ones, along the molecular plane, coincide with the blue absorption (orange color of the crystal). The formation and relative orientation of dimers in the TAAP crystal cause large differences in optical properties in those two perpendicular directions. This explains the relatively large pleochroic effect at the (001) plane of the crystal (Figure 9e). However, at the (100) plane there is no preferential orientation of the molecules with the largest TDMs oriented in one direction, and as such, in every direction there is a strong interaction with the polarized light; thus we observe only a weak pleochroic effect (Figure 9f). This phenomenon is also observed on the absorption spectra of the TAAP; there are three maxima in the visible range corresponding to three observed hues of the crystal.

The observed pleochroic effect coincides with the large birefringence observed on the (001) plane of TAAP. An attempt was made to measure all three refractive indices of the TAAP single crystal using the immersion oil method. This has proven to be a difficult task as the crystals dissolve easily in the selected high refractive index immersion oils (Figure S6). A match was observed in bromoform solution with $n = 1.60$. The remaining two indices were assessed from birefringence measurements (Ehringhaus compensator) and confronted with theoretical LFT calculations[65] (see details in the Supporting Information). TAAP is a rare example of high refractive index material (all $n > 1.5$), which coincides with very high birefringence ($\Delta n > 0.6$) observed for single crystals.

CONCLUSIONS

Combined quantum crystallography and conceptual DFT approaches gave unique insight into the molecular self-assembly of TAAP, the triclinic highly optically anisotropic crystals. Calculations of the aromaticity descriptors for fused rings in TAAP revealed that there is no typical $\pi\cdots\pi$ interaction[24] between the molecules forming the dimer. Fused pyridine and pyrazine rings building a heterocyclic triazaacephenanthrylene system are π-deficient. Geometrical analysis of the ring overlap in the dimer alongside the obtained electrostatic potential distribution, and VSCC placement suggests the possible interaction between the lone pair of the N10B atom and an adjacent pyrazine π-deficient ring. Intermolecular interaction analysis proved that the molecular aggregation favors the formation of the dimer between TAAP molecules. This could explain the difficulties in cocrystallization of TAAP with other components. Adjacent dimers are connected via weak interactions enforcing an alignment of the largest molecular transition dipole moments. The triclinic symmetry of this crystal enforced by its 3D architecture is directly responsible for the observed optical anisotropy. Lack of conventional $\pi\cdots\pi$ interactions between fused ring systems can explain the unusual fluorescence observed alongside the direction perpendicular to the formed dimers. The general empirical rule[25] states that increasing π-overlap causes fluorescence quenching. The example of TAAP forces us to re-examine this rule and pay more attention to the character of the overlapping rings. We should focus specifically on aromaticity descriptors, which can provide insight into the type of the formed interactions. Calculations performed in this work confirmed the dispersive nature of the interactions in the dimer of TAAP, with a strong indication of Lp$\cdots\pi$-deficient ring interaction. In order to disentangle the dispersive interactions into separate contributions, especially important in the fused systems, we would require a new set of quantum chemistry tools.

ASSOCIATED CONTENT

Supporting Information

The Supporting Information is available free of charge at https://pubs.acs.org/doi/10.1021/acs.jpca.9b10651.

Tables of crystal data, aromaticity indicators, bond lengths and angles, bond critical points, refractive indices; figures of dimer structure, electrostatic potential isosurfaces data, local coordinate system, density analysis results, UV–vis spectra, TAAP crystals (PDF)
TAAP crystal data (CIF)

AUTHOR INFORMATION

Corresponding Author

Marlena Gryl − *Faculty of Chemistry, Jagiellonian University, 30-387 Kraków, Poland;* orcid.org/0000-0003-2267-1588; Email: gryl@chemia.uj.edu.pl

Authors

Katarzyna Ostrowska − *Faculty of Chemistry, Jagiellonian University, 30-387 Kraków, Poland;* orcid.org/0000-0002-6425-5331

Jose Enrique Barquera-Lozada − *Instituto de Química, Universidad Nacional Autónoma de México, Circuito exterior, Ciudad Universitaria Coyoacán, México, DF 04510, Mexico;* orcid.org/0000-0002-9668-5328

Katarzyna M. Stadnicka − *Faculty of Chemistry, Jagiellonian University, 30-387 Kraków, Poland;* orcid.org/0000-0002-3898-5824

Complete contact information is available at:
https://pubs.acs.org/10.1021/acs.jpca.9b10651

Author Contributions

The manuscript was written through contributions of all authors. All authors have given approval to the final version of the manuscript.

Notes

The authors declare no competing financial interest.
CCCD reference number: 1965626

ACKNOWLEDGMENTS

REFERENCES

(1) Hollingsworth, M. D. Crystal Engineering: From Structure to Function. *Science* **2002**, *295*, 2410−2413.

(2) Sato, O. Dynamic Molecular Crystals with Switchable Physical Properties. *Nat. Chem.* **2016**, *8*, 644−656.

(3) Guenthner, A. J.; Ramirez, S. M.; Ford, M. D.; Soto, D.; Boatz, J. A.; Ghiassi, K. B.; Mabry, J. M. Organic Crystal Engineering of Thermosetting Cyanate Ester Monomers: Influence of Structure on Melting Point. *Cryst. Growth Des.* **2016**, *16*, 4082−4093.

(4) Gryl, M.; Cenedese, S.; Stadnicka, K. Crystal Engineering and Charge Density Study of Pharmaceutical Nonlinear Optical Material: Melamine-Barbital Co-Crystal. *J. Phys. Chem. C* **2015**, *119*, 590−598.

(5) Lei, B. H.; Yang, Z.; Pan, S. Enhancing Optical Anisotropy of Crystals by Optimizing Bonding Electron Distribution in Anionic Groups. *Chem. Commun.* **2017**, *53*, 2818−2821.

(6) Wojnarska, J.; Gryl, M.; Seidler, T.; Stadnicka, K. M. Crystal Engineering, Optical Properties and Electron Density Distribution of Polar Multicomponent Materials Containing Sulfanilamide. *CrystEngComm* **2018**, *20*, 3638−3646.

(7) Gryl, M.; Seidler, T.; Wojnarska, J.; Stadnicka, K.; Matulková, I.; Němec, I.; Němec, P. Co-Crystals of 2-Amino-5-Nitropyridine Barbital with Extreme Birefringence and Large Second Harmonic Generation Effect. *Chem. - Eur. J.* **2018**, *24*, 8727−8731.

(8) Hong, F.; Jiang, S.; Lan, X.; Narayanan, R. P.; Šulc, P.; Zhang, F.; Liu, Y.; Yan, H. Layered-Crossover Tiles with Precisely Tunable Angles for 2D and 3D DNA Crystal Engineering. *J. Am. Chem. Soc.* **2018**, *140*, 14670−14676.

(9) Bushuyev, O. S.; Friščić, T.; Barrett, C. J. Controlling Dichroism of Molecular Crystals by Cocrystallization. *Cryst. Growth Des.* **2016**, *16*, 541−545.

(10) Ostrowska, K.; Musielak, B.; Szneler, E.; Dudek, Ł.; Gryl, M.; Stadnicka, K. Chelate Ring Size Effect as a Factor of Selective Fluorescent Recognition of Zn2+ Ions by Pyrrolo[2,3-b]quinoxaline with a Substituted 2 Pyridyl Group Receptor. *Inorg. Chem.* **2015**, *54*, 8423−8435.

(11) Etter, M. C. Encoding and Decoding Hydrogen-Bond Patterns of Organic Compounds. *Acc. Chem. Res.* **1990**, *23*, 120−126.

(12) Danel, A.; Wojtasik, K.; Szlachcic, P.; Gryl, M.; Stadnicka, K. A new regiospecific synthesis method of 1H-pyrazolo[3,4-b] quinoxalines e Potential materials for organic optoelectronic devices, and a revision of an old scheme. *Tetrahedron* **2017**, *73*, 5072−5081.

(13) Desiraju, G. R. Crystal Engineering: From Molecule to Crystal. *J. Am. Chem. Soc.* **2013**, *135*, 9952−9967.

(14) Aakeröy, C. B.; Chopade, P. D.; Desper, J. Establishing a Hierarchy of Halogen Bonding by Engineering Crystals without Disorder. *Cryst. Growth Des.* **2013**, *13*, 4145−4150.

(15) Munshi, P.; Venugopala, K. N.; Jayashree, B. S.; Guru Row, T. N. Concomitant Polymorphism in 3-Acetylcoumarin: Role of Weak C-H···O and C-H···π Interactions. *Cryst. Growth Des.* **2004**, *4*, 1105−1107.

(16) Khrustalev, V. N.; Krasnov, K. a.; Timofeeva, T. V. Weak Interactions in Barbituric Acid Derivatives. Unusually Steady Intermolecular Organic "Sandwich" Complexes. Π−π Stacking versus Hydrogen Bonding Interactions. *J. Mol. Struct.* **2008**, *878*, 40−49.

(17) Bauzá, A.; Sharko, A. V.; Senchyk, G. A.; Rusanov, E. B.; Frontera, A.; Domasevitch, K. V. Π-Hole Interactions At Work: Crystal Engineering With Nitro-Derivatives. *CrystEngComm* **2017**, *19*, 1933−1937.

(18) Pavlakos, I.; Arif, T.; Aliev, A. E.; Motherwell, W. B.; Tizzard, G. J.; Coles, S. J. Noncovalent Lone Pair(No-π!)-Heteroarene Interactions: The Janus-Faced Hydroxy Group. *Angew. Chem., Int. Ed.* **2015**, *54*, 8169−8174.

(19) Motherwell, W. B.; Moreno, R. B.; Pavlakos, I.; Arendorf, J. R. T.; Arif, T.; Tizzard, G. J.; Coles, S. J.; Aliev, A. E. Noncovalent Interactions of π Systems with Sulfur: The Atomic Chameleon of Molecular Recognition. *Angew. Chem., Int. Ed.* **2018**, *57*, 1193−1198.

(20) Alonso, M.; Woller, T.; Martín-Martínez, F. J.; Contreras-García, J.; Geerlings, P.; De Proft, F. Understanding the Fundamental Role of Dispersion Interactions in Shaping Carbon-Based Materials. *Chem. - Eur. J.* **2014**, *20*, 4931−4941.

(21) Mooibroek, T. J.; Gamez, P. How Directional Are D-H···phenyl Interactions in the Solid State (D = C, N, O)? *CrystEngComm* **2012**, *14*, 8462−8467.

(22) Frontera, A.; Gamez, P.; Mascal, M.; Mooibroek, T. J.; Reedijk, J. Putting Anion-π Interactions into Perspective. *Angew. Chem., Int. Ed.* **2011**, *50*, 9564−9583.

(23) Jia, C.; Miao, H.; Hay, B. P. Crystal Structure Evidence for the Directionality of Lone Pair − π Interactions − Fact or Fiction? *Cryst. Growth Des.* **2019**, *19*, 6806−6821.

(24) Hunter, Ch.A.; Sanders, J. K. M. The nature of π-interactions. *J. Am. Chem. Soc.* **1990**, *112*, 5525−5534.

(25) Ostrowska, K.; Ceresoli, D.; Stadnicka, K.; Gryl, M.; Cazzaniga, M.; Soave, R.; Musielak, B.; Witek, Ł. J.; Goszczycki, P.; Grolik, J.; et al. π-π-Induced Aggregation and Single-Crystal Fluorescence Anisotropy of 5,6,10b-Triazaacephenanthrylene. *IUCrJ* **2018**, *5*, 335−347.

(26) Srujana, P.; Sudhakar, P.; Radhakrishnan, T. P. Enhancement of Fluorescence Efficiency from Molecules to Materials and the Critical Role of Molecular Assembly. *J. Mater. Chem. C* **2018**, *6*, 9314−9329.

(27) Wang, H.; Zhao, E.; Lam, J. W. Y.; Tang, B. Z. AIE Luminogens: Emission Brightened by Aggregation. *Mater. Today* **2015**, *18*, 365−377.

(28) Genoni, A.; Bučinský, L.; Claiser, N.; Contreras-García, J.; Dittrich, B.; Dominiak, P. M.; Espinosa, E.; Gatti, C.; Giannozzi, P.; Gillet, J. M. Quantum Crystallography: Current Developments and Future Perspectives. *Chem. - Eur. J.* **2018**, *24* (43), 10881−10905.

(29) Hansen, N. K.; Coppens, P. Testing aspherical atom refinements on small-molecule data sets. *Acta Crystallogr., Sect. A: Cryst. Phys., Diffr., Theor. Gen. Crystallogr.* **1978**, *34*, 909−921.

(30) Bader, R. F. W. *Atoms in Molecules. A Quantum Theory*; Clarendon Press: Oxford, UK, 1990.

(31) Turner, M. J.; McKinnon, J. J.; Wolff, S. K.; Grimwood, D. J.; Spackman, P. R.; Jayatilaka, D.; Spackman, M. A. *CrystalExplorer17*; University of Western Australia, 2017; http://hirshfeldsurface.net.

(32) De Proft, F.; Geerlings, P. Conceptual and Computational DFT in the Study of Aromaticity. *Chem. Rev.* **2001**, *101* (5), 1451−1464.

(33) Ziegler, T.; Rauk, A. On the calculation of bonding energies by the Hartree−Fock Slater method. *Theoretica Chimica Acta* **1977**, *46*, 1−10.

(34) Luong, T. M.; Pilkington, L. I.; Barker, D. Stereoselective Total Synthesis of (+)-Aristolactam GI. *J. Org. Chem.* **2019**, *84* (9), 5747−5756.

(35) Ostrowska, K.; Dudek, K.; Musielak. Synthesis of the new heterocyclic system 5,6,10b-triazaacephenanthrylene, a nitrogen analogue of aristolactams. *Heterocycles* **2016**, *92*, 1307−1312.

(36) Keith, T. A.. *AIMAll*, Version 19.10.12; TK Gristmill Software: Overland Park, KS, USA, 2019 (aim.tkgristmill.com).

(37) Frisch, M. J.; Trucks, G. W.; Schlegel, H. B.; Scuseria, G. E.; Robb, M. A.; Cheeseman, J. R.; Scalmani, G.; Barone, V.; Petersson, G. A.; Nakatsuji, H.; Li, X.; Caricato, M.; Marenich, A. V.; Bloino, J.; Janesko, B. G.; Gomperts, R.; Mennucci, B.; Hratchian, H. P.; Ortiz, J. V.; Izmaylov, A. F.; Sonnenberg, J. L.; Williams-Young, D.; Ding, F.; Lipparini, F.; Egidi, F.; Goings, J.; Peng, B.; Petrone, A.; Henderson, T.; Ranasinghe, D.; Zakrzewski, V. G.; Gao, J.; Rega, N.; Zheng, G.; Liang, W.; Hada, M.; Ehara, M.; Toyota, K.; Fukuda, R.; Hasegawa, J.; Ishida, M.; Nakajima, T.; Honda, Y.; Kitao, O.; Nakai, H.; Vreven, T.; Throssell, K.; Montgomery, J. A., Jr.; Peralta, J. E.; Ogliaro, F.; Bearpark, M. J.; Heyd, J. J.; Brothers, E. N.; Kudin, K. N.; Staroverov, V. N.; Keith, T. A.; Kobayashi, R.; Normand, J.; Raghavachari, K.; Rendell, A. P.; Burant, J. C.; Iyengar, S. S.; Tomasi, J.; Cossi, M.; Millam, J. M.; Klene, M.; Adamo, C.; Cammi, R.; Ochterski, J. W.; Martin, R. L.; Morokuma, K.; Farkas, O.; Foresman, J. B.; Fox, D. J. *Gaussian 16*, Revision C.01; Gaussian, Inc.: Wallingford, CT, 2016.

(38) Zheng, J.; Zhao, Y.; Truhlar, D. G. Representative Benchmark Suites for Barrier Heights of Diverse Reaction Types and Assessment of Electronic Structure Methods for Thermochemical Kinetics. *J. Chem. Theory Comput.* **2007**, *3* (2), 569−582.

(39) Dovesi, R.; Erba, A.; Orlando, R.; Zicovich-Wilson, C. M.; Civalleri, B.; Maschio, L.; Rerat, M.; Casassa, S.; Baima, J.; Salustro, S.; Kirtman, B. *WIREs Comput. Mol. Sci.* **2018**, *8*, No. e1360.

(40) Dovesi, R.; Saunders, V. R.; Roetti, C.; Orlando, R.; Zicovich-Wilson, C. M.; Pascale, F.; Civalleri, B.; Doll, K.; Harrison, N. M.; Bush, I. J.; D'Arco, P.; Llunell, M.; Causà, M.; Noël, Y.; Maschio, L.; Erba, A.; Rerat, M.; Casassa, S. *CRYSTAL17 User's Manual*; University of Torino: Torino, 2017.

(41) Volkov, A.; Macchi, P.; Farrugia, L. J.; Gatti, C.; Mallinson, P.; Richter, T.; Koritsanszky, T. *XD2006: A computer program for multipole refinement, topological analysis of intermolecular energies from experimental and theoretical structure factors*; http://xd.chem.buffalo.edu/

(42) Meindl, K.; Henn, J. Foundations of Residual-Density Analysis. *Acta Crystallogr., Sect. A: Found. Crystallogr.* **2008**, *64* (3), 404−418.

(43) Abramov, Y. A. On the Possibility of Kinetic Energy Density Evaluation from the Experimental Electron-Density Distribution. *Acta Crystallogr., Sect. A: Found. Crystallogr.* **1997**, *53* (3), 264−272.

(44) Espinosa, E.; Molins, E.; Lecomte, C. Hydrogen bond strengths revealed by topological analyses of experimentally observed electron densities. *Chem. Phys. Lett.* **1998**, *285*, 170−173.

(45) Johnson, E. R.; Keinan, S.; Mori-Sanchez, P.; Contreras-Garcia, J.; Cohen, A. J.; Yang, W. Revealing Noncovalent Interactions. *J. Am. Chem. Soc.* **2010**, *132*, 6498−6506.

(46) Contreras-Garcia, J.; Johnson, E. R.; Keinan, S.; Chaudret, R.; Piquemal, J.-P.; Beratan, D. N.; Yang, W. *J. Chem. Theory Comput.* **2011**, *7*, 625−632.

(47) Ziegler, T.; Rauk, A. On the calculation of bonding energies by the Hartree−Fock Slater method. *Theoretica Chimica Acta* **1977**, *46*, 1−10.

(48) Fonseca Guerra, C.; Snijders, J. G.; Velde, G.; Baerends, E. J. Regular Article Towards an Order- N DFT Method. *Theor. Chem. Acc.* **1998**, *99* (6), 391−403.

(49) te Velde, G.; Bickelhaupt, F. M.; Baerends, E. J.; Fonseca Guerra, C.; van Gisbergen, S. J. A.; Snijders, J. G.; Ziegler, T. Chemistry with ADF. *J. Comput. Chem.* **2001**, *22* (9), 931−967.

(50) *ADF2013*; SCM, Theoretical Chemistry, Vrije Universiteit: Amsterdam, The Netherlands, http://www.scm.com.

(51) Grimme, S.; Antony, J.; Ehrlich, S.; Krieg, H. A Consistent and Accurate Ab Initio Parametrization of Density Functional Dispersion Correction (DFT-D) for the 94 Elements H-Pu. *J. Chem. Phys.* **2010**, *132* (15), 154104.

(52) Alonso, M.; Pinter, B.; Woller, T.; Geerlings, P.; De Proft, F. Scrutinizing Ion-π and Ion-σ Interactions Using the Noncovalent Index and Energy Decomposition Analysis. *Comput. Theor. Chem.* **2015**, *1053*, 150−164.

(53) Giambiagi, M.; De Giambiagi, M. S.; Dos Santos Silva, C. D.; De Figueiredo, A. P. Multicenter Bond Indices as a Measure of Aromaticity. *Phys. Chem. Chem. Phys.* **2000**, *2* (15), 3381−3392.

(54) Bultinck, P.; Ponec, R.; Van Damme, S. Multicenter Bond Indices as a New Measure of Aromaticity in Polycyclic Aromatic Hydrocarbons. *J. Phys. Org. Chem.* **2005**, *18* (8), 706−718.

(55) Feixas, F.; Matito, E.; Poater, J.; Solà, M. Quantifying Aromaticity with Electron Delocalisation Measures. *Chem. Soc. Rev.* **2015**, *44* (18), 6434−6451.

(56) Zhao, Y.; Truhlar, D. G. The M06 suite of density functionals for main group thermochemistry, thermochemical kinetics, non-covalent interactions, excited states, and transition elements: two new functionals and systematic testing of four M06-class functionals and 12 other functionals. *Theor. Chem. Acc.* **2008**, *120*, 215−241.

(57) Barquera-Lozada; Vorticity, J. E. Simplifying the analysis of the current density. *J. Comput. Chem.* **2019**, *40*, 2602.

(58) Barquera-Lozada, J. E. The vorticity of the current density tensor and 3D-aromaticity. *Int. J. Quantum Chem.* **2019**, *119*, No. e25848.

(59) Sundholm, D.; Fliegl, H.; Berger, R. J. F. Calculations of magnetically induced current densities: theory and applications. *Wiley Interdiscip. Rev. Comput. Mol. Sci.* **2016**, *6*, 639.

(60) Gershoni-Poranne, R.; Stanger, A. Magnetic criteria of aromaticity. *Chem. Soc. Rev.* **2015**, *44*, 6597.

(61) Steiner, E.; Fowler, P. W. Four- and two-electron rules for diatropic and paratropic ring currents in monocyclic π systems. *Chem. Commun.* **2001**, 2220.

(62) Fowler, P. W.; Steiner, E.; Havenith, R. W. A.; Jenneskens, L. W. Current density, chemical shifts and aromaticity. *Magn. Reson. Chem.* **2004**, *42*, S68−78.

(63) Stalke, D. *Electron Density and Chemical Bonding II*; Springer, 2012.

(64) Liegeois, V. *DrawMol*; UNamur, www.unamur.be/drawmol.

(65) Seidler, T.; Stadnicka, K.; Champagne, B. Evaluation of the Linear and Second-Order NLO Properties of Molecular Crystals within the Local Field Theory: Electron Correlation Effects, Choice of XC Functional, ZPVA Contributions, and Impact of the Geometry in the Case of 2-Methyl-4-Nitroaniline. *J. Chem. Theory Comput.* **2014**, *10* (5), 2114−2124.